Received: 14 March 2018 | Revised: 12 June 2018 | Accepted: 14 June 2018

DOI: 10.1002/gj.3283

RESEARCH ARTICLE

WILEY

The significance of early Permian and early Carboniferous U–Pb zircon ages in the Bossòst and Lys-Caillaouas granitoids (Pyrenean Axial Zone)

Marco A. Lopez-Sanchez[1] | Joaquín García-Sansegundo[1] | Francisco J. Martínez[2]

[1] Departamento de Geología, Universidad de Oviedo, Oviedo, Spain

[2] Departament de Geologia, Universitat Autònoma de Barcelona, Bellaterra, Spain

Correspondence
Marco A. Lopez-Sanchez, Géosciences Montpellier, Université de Montpellier & CNRS, Campus Triolet CC 060, Place Eugène Bataillon, 34095 Montpellier Cedex 05, France.
Email: marco-antonio.lopez-sanchez@umontpellier.fr

Present Address
Marco A. Lopez-Sanchez, Géosciences Montpellier, Université de Montpellier & CNRS, Campus Triolet CC 060, Place Eugène Bataillon, 34095 Montpellier Cedex 05, France.

Funding information
Spanish Ministry for Science and Innovation, Grant/Award Number: CGL2006-08822/BTE

Handling Editor: P. Lancaster

The Axial Zone of the Alpine Pyrenees exposes Ediacaran-Palaeozoic metasediments and orthogneisses intruded by abundant Variscan granitoids that resulted in elongated HT metamorphic domes separated by tight synforms with low-grade metasediments. Yet, the age of the granitoids within the metamorphic domes remains debated, hindering the correlation of Variscan deformation stages and the HT metamorphism between the different domes. Here, we dated two granitoids located within classical metamorphic domes using U–Pb LA-ICP-MS zircon geochronology: the Bossòst and the Lys-Caillaouas granitoids in the Garona and Lys-Caillaouas domes, respectively. The results indicate that the leucogranitic facies of both granitoids have Early Permian crystallization ages at 295 ± 2 Ma and 297 ± 2 Ma, respectively. Furthermore, we found a small population of inherited zircon with Serpukhovian (331–323 Ma) ages in the Lys-Caillaouas granitoid, reinforcing the existence of an elusive but widespread early Carboniferous magmatic event in the Pyrenees. These ages discard two previous hypotheses explaining the age disparity observed in the different domes: either that the HT-LP metamorphism is of Visean age only or that the dome formation was diachronous along the Axial Zone, ranging from Visean in the central part to late Carboniferous in the eastern Axial Zone. The early Permian age found in the leucogranitic facies of the Bossòst granitoid questions the proposed Visean age for the formation of the Garona dome and the peak HT-LP metamorphism and points to an Early Permian age as most likely in line with what is observed in the Lys-Caillaouas Massif.

KEYWORDS

granitoids, HT-LP metamorphism, metamorphic domes, Pyrenees, U–Pb age, Variscan

1 | INTRODUCTION

Isotopic dating in granitoids alongside their relationship with the host rocks are key to constraining the age of deformation stages in metamorphic terranes (Paterson & Tobisch, 1988; Paterson, Tobisch, & Vernon, 1989). In the Pyrenees mountain range, a kilometre-scale Alpine antiformal stack exposes at its core the basement, often referred to as the Pyrenean Axial Zone (Figure 1). This zone is composed by Ediacaran-Palaeozoic metasediments and orthogneisses intruded by a large number of Variscan granitoids. Structurally, the Axial Zone is characterized by a polyphase Variscan deformation that resulted in elongated *HT* metamorphic domes that follow the trend of the Pyrenean belt separated by tight synforms with low-grade metasediments (e.g., Carreras & Capella, 1994). Despite the large number of tectonometamorphic studies since the 1960s, two main problems remain unsolved: how and when the metamorphic domes were formed.

The Variscan deformation in the western and southern parts of the Axial Zone is characterized by folds associated with south-directed

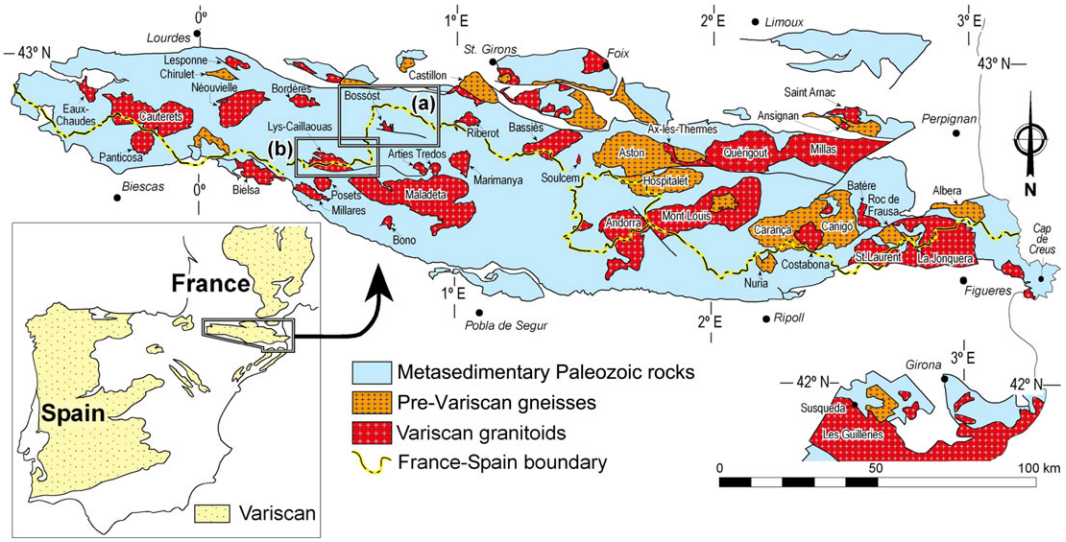

FIGURE 1 Geological map of the Axial Zone of the Pyrenees showing the location of the Bossòst (a) and Lys-Caillaouas (b) metamorphic domes. In the bottom right, the map of the Catalonian Coastal Ranges [Colour figure can be viewed at wileyonlinelibrary.com]

thrusts and a low grade or lack of metamorphism. The domes reveal the deepest levels of the Variscan crust in which median to high-grade metasediments, orthogneisses, and granitoids outcrop. Three main foliations characterize the Variscan deformation. The first two are related to folds and thrusts developed at low-grade conditions, whereas the third is related to shear zones developed under LP-HT conditions (García-Sansegundo, Poblet, Alonso, & Clariana, 2011). The Alpine deformation has minor effects in the Variscan structure and includes thrusts with a general top-to-the-south movement, producing a local change of attitude and tightening of Variscan folds (e.g., Gutiérrez-Medina, Alonso, & García-Sansegundo, 2012; Mey, 1968), and the local development of foliations in the absence of metamorphism and magmatism.

The LP-HT metamorphism is restricted to the metamorphic domes and has been attributed to the intrusion of the so-called deep-seated granitoids (e.g., Carreras & Capella, 1994). The main feature of such granitoids is the lack of well-defined narrow contact aureoles, outcropping within wide areas where staurolite, cordierite, and/or andalusite assemblages and migmatization appear (e.g., Autran, Fonteilles, & Guitard, 1970; Mezger & Passchier, 2003; Mezger & Regnier, 2016). Representative examples are the Cap de Creus pegmatites, granitoids of Canigó-Carança Massif, and the Lys-Caillaouas, Ax-les-Thermes, Soulcen, and Bossòst granitoids (Figure 1).

Among all the different tectonic models previously proposed for the origin of the domes (e.g., Carreras & Capella, 1994 and references therein), two main opposing views persist nowadays. Some authors propose that the domes, the flat-lying schistosity, and HT-LP metamorphism formed under an extensional regime, although there is disagreement about the timing of this event during the Variscan cycle (e.g., Aerden, 1994; Kriegsman, Aerden, Bakker, Denbrok, & Schutjens, 1989; Mezger & Gerdes, 2016; Mezger & Passchier, 2003; Van Den Eeckhout & Zwart, 1988; Vissers, 1992). Others propose a dextral transpressive regime during the dome formation (Carreras & Capella, 1994; Esteban et al., 2015). The authors supporting a transpressive regime usually cite as evidence the attitude of magnetic fabrics and mineral lineation in the granites, which are arranged subhorizontal and slightly oblique to the Variscan trend in the Axial Zone. However, the oblique and subhorizontal arrangement of structures has also been related to extensional detachments in other parts of the Variscan orogen in Western Europe (e.g., Lopez-Sanchez, Marcos, Martínez, Iriondo, & Llana-Fúnez, 2015 and references therein), making this criterion ambiguous. Lastly, some authors have taken an intermediate position on this matter, stating that some domes would have been formed due to a local extension in a broad transpressive regime (Denèle et al., 2014; Mezger, 2009).

Despite these significant differences, there is also consensus on some of the features that characterize the domes. For example,

(i) the dome-shaped structure was essentially formed during the Variscan cycle, although some domes could be accentuated by Alpine tectonics;

(ii) the formation of flat-lying schistosities was coeval with the development of HT-LP metamorphism; and

(iii) the development of a HT-LP metamorphism and migmatization was coeval with the emplacement of the so-called deep-seated granitoids.

Due to the aforementioned features, there is a lot of interest in dating the plutons linked with the HT-LP metamorphism. This will allow correlating the metamorphism and structures across the different metamorphic domes and ultimately help to understand their origin. Unfortunately, most of these "deep-seated" granitoids lack reliable dating because they contain many inherited zircon grains (e.g., Denèle et al., 2014). Indeed, the "deep-seated" granitoids have provided two well-differentiated isotopic ages using U–Pb zircon/monazite dating:

(i) Late Carboniferous ages. An age of 306 ± 2 Ma (U–Pb LA-ICP-MS) found by Denèle et al. (2014) in the Ax-les-Thermes granitoid (Aston dome), and another of 300 ± 2 Ma (U–Pb SIMS

SHRIMP) by Esteban et al. (2015) in two facies of the Lys-Caillaouas granitoid (Lys-Caillaous Massif).

(ii) Early Carboniferous (Visean) ages of ca. 337–339 Ma (U–Pb LA-ICP-MS) found by Mezger and Gerdes (2016) in the Saulcen (Aston dome) and different facies of the Bossòst granitoids (Garona Dome).

The disagreement in the age of emplacement of these granitoids is odd since it is always related to similar deformation and metamorphic events along the Axial Zone (Denèle et al., 2014; Hilario, 2004; Mezger & Passchier, 2003; Mezger & Gerdes, 2016). The late Carboniferous ages agree with the well-known late- to post-orogenic magmatism observed through the entire Variscan belt and well documented in the Pyrenees (Denèle et al., 2014; Druguet, Castro, Chichorro, Francisco Pereira, & Fernandez, 2014; Evans, Gleizes, Leblanc, & Bouchez, 1998; Gleizes, Crevon, Asrat, & Barbey, 2006; Martínez et al., 2016; Maurel, Respaut, Monie, Arnaud, & Brunel, 2004; Paquette, Gleizes, Leblanc, & Bouchez, 1997; Pereira et al., 2014; Roberts, Pin, Clemens, & Paquette, 2000; Romer & Soler, 1995). Zircon and monazite grains with early Carboniferous ages have also been found in some granitoids in the Pyrenees (Denèle, 2007; Denèle et al., 2014; Mezger & Gerdes, 2016), but the significance of these ages is still controversial. For example, Denèle et al. (2014) concluded that zircon grains with early Carboniferous ages in the Ax-les-Thermes granitoid are artefacts due to mixing ages and only late Carboniferous and pre-Silurian ages have geological significance. However, the zircon age clusters found by Mezger and Gerdes (2016) in the Bossòst and Saulcen granitoids are tight and formed by many zircon grains (>10), being the probability of finding such tight clusters by chance negligible. Accordingly, we think that the mixing age hypothesis proposed by Denèle et al. (2014) cannot be generalized for the entire Axial Zone and that some zircon grains truly record an early Carboniferous magmatic event.

It should be also added that zircon and monazite grains with early Carboniferous ages (ca. 320 Ma), considered either as xenocryst (i.e., inherited crystals) or as syn-magmatic, have been found in other metamorphic domes in the adjacent Variscan massifs (e.g., Gutiérrez-Alonso, Fernández-Suárez, López-Carmona, & Gärtner, 2018; López-Moro et al., 2018; Martínez et al., 2016; Martínez, Reche, & Iriondo, 2008; Poilvet, Poujol, Pitra, Van Den Driessche, & Paquette, 2011). A particularly well-documented case is the Tormes Dome in the Iberian Massif, where the limited overprint of the widespread late Carboniferous–early Permian magmatism allowing to recognize several igneous rocks with an unequivocal early Carboniferous age (López-Moro et al., 2018). Overall, these examples support the existence of an early Carboniferous magmatic event in some areas during Variscan times. Its effect, however, seems to be obscured due to the overprinting of the widespread late Carboniferous–early Permian magmatic event.

With the current state of affairs, two interpretations are possible in relation to the timing of the formation of the metamorphic domes in the Axial Zone:

(i) Domes formed at different stages of the Variscan cycle and cannot be correlated in time despite showing a similar sequence of tectonic and metamorphic events.

(ii) All the domes and related metamorphism formed contemporarily, and the geological meaning of one of the two different Variscan zircon ages is misinterpreted.

To shed some light on this matter, we dated the Bossòst and the Lys-Caillaouas granitoids, both located in different domes with similar structural relations with the host rocks but, strikingly, different emplacement ages. In both, the samples were collected in facies that have not been previously dated.

2 | GEOLOGICAL SETTING

The Bossòst and Lys-Caillaouas granitoids outcrop in the central part of the Pyrenees, the Bossòst granitoid in the southern part of the Garona Dome and the Lys-Caillaouas granitoid farther south, in the Lys-Caillaouas Massif (Figures 1 and 2). Both granitoids emplaced in a Cambro-Ordovician sequence, the Jujols Series (Cavet, 1957), composed by quartzite, slates and interbedded limestones, and outcrop within areas of HT-LP metamorphism (García-Sansegundo & Alonso, 1989; García-Sansegundo, Martín-Izard, & Gavaldà, 2014; Kriegsman et al., 1989). Overlying these series, there are late Ordovician slates, sandstones, conglomerates and limestone, and Silurian bituminous slates (García-Sansegundo, Gavaldà, & Alonso, 2004). Between both domes, the Aran Valley Synclinorium exposes more than 1,000 m of slates, limestones, sandstones, and quartzites of Devonian age (García-López, García-Sansegundo, & Arbizu, 1991; García-Sansegundo, 1992; Kleinsmiede, 1960), which is locally affected by the HT-LP metamorphism (Figure 2).

2.1 | Structure and metamorphism of the host rocks

Four main Pre-Alpine deformation phases affect the metamorphic rocks of the Garona and Lys-Caillaouas metamorphic domes:

- A pre-Variscan south-verging cleavage (S_E) with no folds associated. This foliation appears solely in the Cambro-Ordovician rocks that lie under the upper Ordovician unconformity and has been linked to/with the development of extensional pre-Silurian faults in the area (Casas, 2010; García-Sansegundo et al., 2004; García-Sansegundo et al., 2011; García-Sansegundo et al., 2014).
- D1 structures consisting of north-verging E-W recumbent or inclined folds with an associated horizontal foliation (S_1). These structures are best developed in the metamorphic domes (Garona and Lys-Caillaouas massifs), being S_1 the dominant foliation, and fade out toward shallower levels in the Aran Valley Synclinorium (García-Sansegundo, 1992, 1996; García-Sansegundo et al., 2014; García-Sansegundo & Alonso, 1989; Kriegsman et al., 1989). The foliation S_1 appears as a slaty cleavage in the Upper Ordovician-Devonian sequence and as a crenulation cleavage in the places where the previous S_E foliation developed (Clariana & García-Sansegundo, 2009; García-Sansegundo et al., 2011).
- D2 structures consist of south-directed thrusts with associated E-W upright folds affecting D1 structures. The thrusts are detached on Silurian shales and the Cambro-Ordovician sequence.

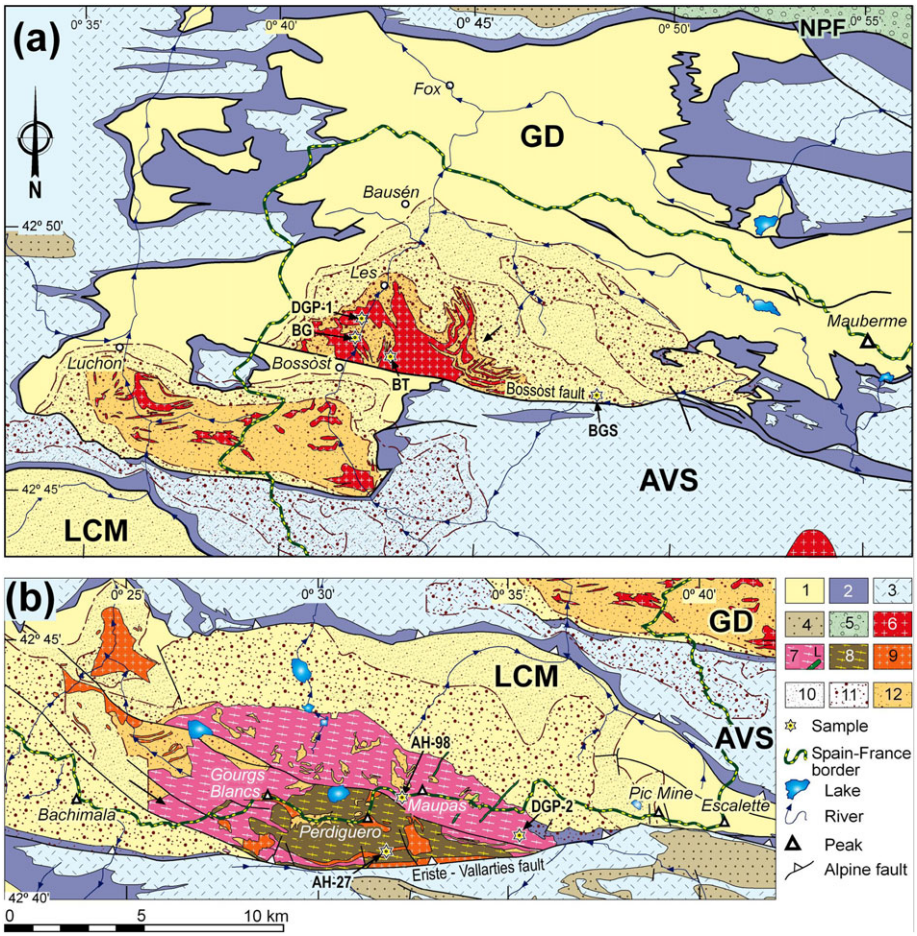

FIGURE 2 Detailed maps and sample locations. (a) Geological map of the Garona dome with the location sample DGP-1 (this study) and samples BG, BT, and BGS of Mezger and Gerdes (2016). (b) Geological map of the Lys Caillaouas Massif with the location of sample DGP-2 (this study) and samples AH-27 and AH-98 of Esteban et al. (2015). NPF: North-Pyrenean Fault; GD: Garona Dome; AVS: Aran Valley Synclinorium; LCM: Lys-Caillaouas Massif; 1: Cambro-Ordovician rocks; 2: Silurian shales; 3: Devonian series; 4: syn-orogenic Carboniferous series (Culm); 5: Mesozoic cover. Bossòst granitoid, 6: Leucogranites and pegmatites. Lys-Callaouas granitoid, 7: porphyritic granodiorite (L, lamprophyre); 8: quartz-diorite; 9: leucogranite. Metamorphic zones, 10: Biotite zone; 11: Andalusite-Staurolite-Cordierite zone; 12 Sillimanite zone. Geological maps modified from Clin et al. (1986), García-Sansegundo (1992), García-Sansegundo and Ramírez Merino (2013), and Kriegsman et al. (1989) [Colour figure can be viewed at wileyonlinelibrary.com]

Folds with a pervasive crenulation lineation dominate below the detachment level placed in the Silurian shales, while a crenulation cleavage (S_2) dominates above this detachment in the Aran Valley Synclinorium (García-Sansegundo, 1990, 1992, 1996; Matte, 1969).

- D3 structures correspond to shear zones with variable thickness (3–5 km) developed around the deep-seated igneous bodies. The foliation (S_3) associated lies almost parallel to the S_1, making its distinction difficult. Based on a detailed porphyroblast-matrix relation study, Mezger and Passchier (2003) correlated in a single event the development of D3 extensional shear zones, the intrusion of the Bossòst granitoid, and the peak of the LP-HT metamorphism in the Garona Dome.

Two large faults with an E-W direction limit the dated granitoids to the south, the Bossòst Fault in the Garona dome and the Eriste-Vallartiés Fault in the Lys-Caillaouas Massif (Figure 2). Both faults are interpreted to have started their tectonic history during the development of D2 structures (García-Sansegundo, 1992; Hilario, 2004; Pérez Cáceres & García-Sansegundo, 2012). However, both granitoids contain mylonites near these faults, indicating that they were also active after the granite crystallization, even during the Alpine cycle.

The emplacement of the Lys-Caillaouas and Bossòst granitoids are spatially related to a LP-HT metamorphism (M2) that overprints a previous greenschist- to amphibolite-facies metamorphism (M1). In both domes, the LP-HT metamorphism developed around the intrusions, where it can be recognized a prograde zoning with biotite, staurolite-andalusite-cordierite, and sillimanite-cordierite towards the contact with the granitoids (Clin, 1964; Kriegsman et al., 1989; Zwart, 1963, 1979). The granitoids never cut the LP-HT metamorphic zonation (i.e., the isograds). The absence of garnet and the abundance of cordierite are typical. In the Lys-Caillaouas Massif, staurolite is absent due to a high Mg/(Fe + Mg) ratio in the host rocks (Kriegsman et al., 1989). In the Garona Dome, the growth of staurolite overprints the S_1 and S_2 foliations, while andalusite and cordierite grew during the development of D3 extensional shear zones (Mezger & Passchier, 2003).

3 | SHAPE AND PREVIOUS AGES IN THE BOSSÒST AND LYS-CAILLAOUAS GRANITOIDS

The Bossòst granitoid (Figure 2a) mainly consists of granites, leucogranites, and pegmatites arranged subparallel to the dominant S_1 foliation (Figure 2a). Small pegmatitic sills and veins outcrop bordering the main body, whereas the granite appears homogeneous in the central part. The granites are fine- to medium-grained, although locally they appear coarse-grained along with an increase in K-feldspar content (Figure 3a). The major constituents are quartz, albite, K-feldspar, muscovite, and, sometimes, biotite. Apatite, garnet, fibrolite, and zircon appear as accessory minerals. Cordierite, tourmaline, and beryl occur occasionally. Mezger and Gerdes (2016) obtained the following Laser Ablation U–Pb zircon ages: 338 ± 3 Ma (n = 11) in the muscovite granite, 337 ± 2 Ma (n = 27) in a granite sill, and 329 ± 4 Ma (n = 4) in the tonalitic facies (samples BG, BGS, and BT in Figure 2a, respectively). They consider the first two as the age of crystallization.

The Lys-Caillaouas granitoid outcrops in the southern part of the Lys Caillaouas Massif, with the Eriste-Vallartiés Fault cutting across the granitoid southwards (Figure 2b). The granitoid consists of three main facies (Clin, 1964; Clin et al., 1986): (i) porphyritic granodiorites that occur as lenticular bodies with oriented quartz, phyllosilicates, albite, large K-feldspars, and biotite; (ii) homogeneous coarse-grained quartz diorites with feldspar, hornblende, and biotite; and (iii) fine-grained leucogranites that occur in lenticular bodies subparallel to the dominant foliation S_1. In contrast to the Bossòst granitoid, the Lys-Caillaouas granitoid has a laccolithic shape subparallel to the S1 foliation, and the occurrence of large xenoliths is very common (Figure 3b). Esteban et al. (2015) obtained three different SIMS U–Pb zircon ages: 300 ± 2 Ma (n = 17) and 307 ± 3 Ma (n = 11) both in the porphyritic granodiorites facies and 299 ± 1 Ma (n = 8) in the quartz diorites (samples

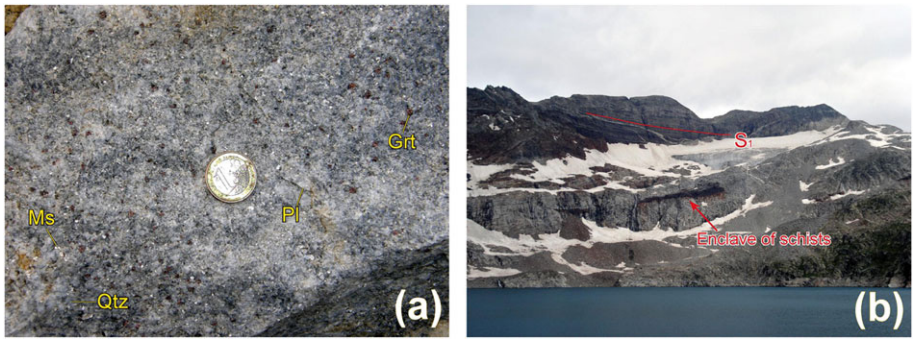

FIGURE 3 (a) The aspect of the Bossòst granitoid in the quarry south of Les. (b) The aspect of the Lys-Caillaouas granitoid. Notice the xenoliths with the S1 cleavage. Abbreviations: Grt - garnet, Ms - muscovite, Pl - plagioclase, Qtz - quartz. Scale: coin 2.5 cm diameter [Colour figure can be viewed at wileyonlinelibrary.com]

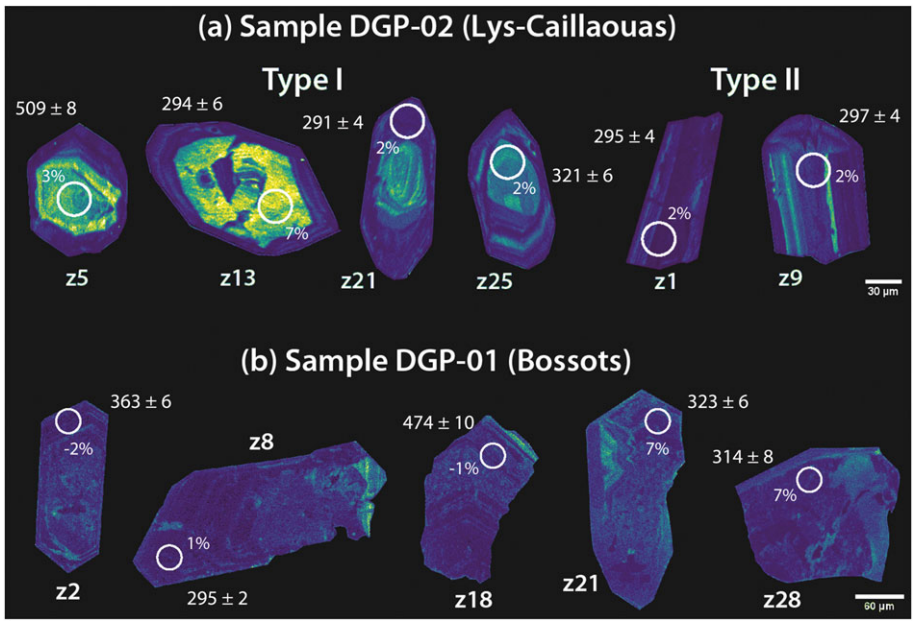

FIGURE 4 SEM-CL image of representative zircon grains from samples DGP-01 and 02. Circles represent the spot size and the location. The ages are reported in million years at the 2σ level of precision. Zircon adjacent numbers represent the spot number and the percentage of discordance, respectively [Colour figure can be viewed at wileyonlinelibrary.com]

AH-98 and AH-27 in Figure 2b, respectively). They consider the 300 ± 2 Ma age as the age of granitoid emplacement.

4 | SAMPLE AND ANALYTICAL METHODS

Sample DGP-01 (Bossòst granitoid) was collected on the western bank of the Garona River located in the south-west of the Les village, where this granitoid is quarried as an ornamental rock (42°48′08.4″N, 0°41′54.2″E; Figure 2b). The sample is a fresh undeformed leucogranite. Sample DGP-02 (Lys-Caillaouas granitoid) was collected in the Remuñe stream, located on the western bank of the Benasque valley (42°41′08.3″N, 0°34′55.5″E; Figure 2b). The sample corresponds to a fresh undeformed porphyritic granodiorite. In both cases, about 10 kg of rock were collected.

Zircon grains were extracted from rock samples using conventional mineral separation methods at Centro de Geociencias in Universidad Autónoma de México (UNAM). Zircon standard Plešovice (337 Ma; Sláma et al., 2008) plus unknowns were mounted in epoxy, ground to nearly half thickness, and polished with 6 and 1 μm grit diamond suspension abrasive, later cleaned in distilled water and 1 N HCl, and gold-coated for maximum surface conductivity. CL images were acquired with a JEOL 5600 SEM at Denver University and enhanced using the ImageJ application (Schneider, Rasband, & Eliceiri, 2012).

Zircon grains from both samples were dated following the method described in Solari, Gomez-Tuena, Pablo Bernal, Perez-Arvizu, and Tanner (2010) using the laser-ablation inductively coupled plasma mass spectrometry (LA-ICP-MS) U (Th)–Pb analysis at the Isotopic Studies Laboratory in UNAM. Briefly, a 30-sec ablation was used, producing a circular sample area of about 33 μm in diameter and 25 μm in depth. For the closest possible control of the measured Pb/U ratios, U, and Th, the analysis sequence started measuring a glass standard NIST SRM 612 (~38 ppm U). This is followed by five zircon analyses of the Plešovice standard, five unknowns, and thereafter another zircon standard for each five unknowns, finishing with two analysis of zircon standard plus one of NIST SRM 612 standard (Gehrels, Valencia, & Ruiz, 2008; Jackson, Longerich, Dunning, & Fryer, 1992; Solari et al., 2010). The LA-ICP-MS data were reduced using the application UPb.

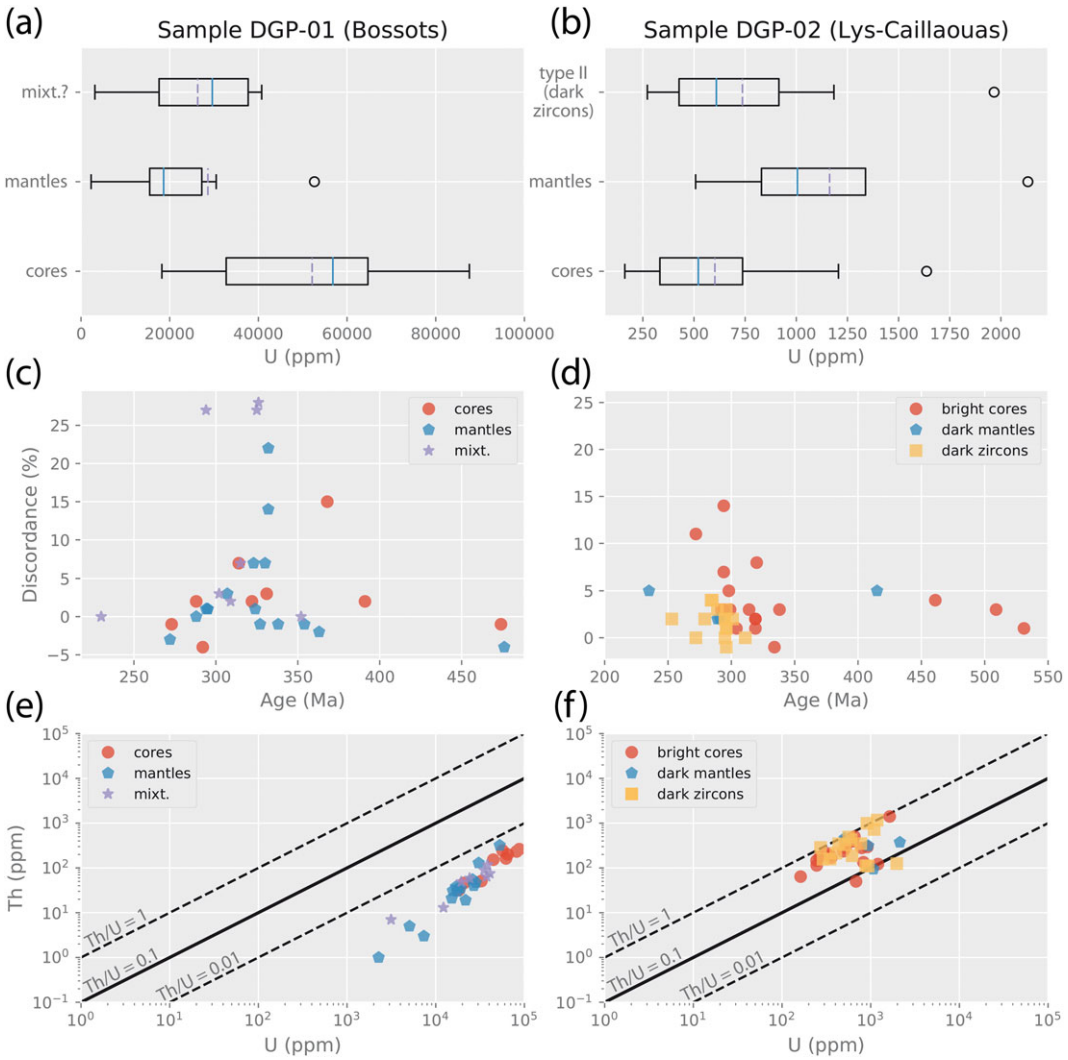

FIGURE 5 Plots showing features of the different zircon domains from the studied samples. (a and b) Box plots showing the U-content in different zircon domains. Solid and dashed lines indicate the median and the mean values, respectively. Boxes are the interquartile range (IQR), whiskers the 1.5 * IQR range and empty dots outliers. Outliers with extreme values were cut for clarity. (c and d) Discordance versus age plots. (e and f) Th versus U content plots [Colour figure can be viewed at wileyonlinelibrary.com]

age (Solari & Tanner, 2011) and plotted using the software Isoplot/Ex 4.15 (Ludwig, 2012). The ratios were corrected offline for common Pb, using the algebraic approach proposed in Andersen (2002). U–Pb age data for zircon were plotted on Wetherill (1956) charts along with a model common Pb line based on Stacey and Kramers (1975), and U–Pb ages calculated using Concordia and Concordia-Intercept ages.

5 | RESULTS

5.1 | Sample DGP-01: Bossòst granitoid

Cathodoluminescence (CL) images show euhedral zircon grains with double-ended prismatic shapes when unbroken (Figure 4b). Zircon grains have dark cores with a notable mottled patchy texture, occasionally showing an oscillatory zoning. The mantles surrounding the cores (e.g., z2, z8, and z28 in Figure 4b) are usually darker with an oscillatory zoning, although with some exceptions (e.g., z28 in Figure 4b). We made 33 analyses with 25 lying within the ±5% of discordance, 9 in the mottled cores, 15 in the mantles, and the rest are suspected of containing parts of the core and the mantle (Figure 5 c, see Table 1). Zircon grains have an unusually high U-content. This is very notable in the mottled dark cores, with a median of 56,800 ppm and values up to 90,000 rather common (Figure 5a). The dark mantles have a lower uranium content, with a median of 18,630 ppm, and leaving aside two outliers (z24 and z31), values are below 30,000 ppm (Figure 5a). Both the cores and the mantles have very low Th/U values (<0.006), more typical of metamorphic zircon (≪0.1; Figure 5e). Although the dispersion of individual zircon ages is wider in the cores than in the mantles, the age range completely overlaps.

The Wetherill plot displays a complex age pattern, with a great dispersion of ages between ca. 260 and 360 Ma (Figures 5c and 6). Only one tight concordant cluster exists. The cluster, formed by three analyses performed in the zircon mantles, yields a concordia age of 295 ± 2 Ma (n = 3; 2-sigma: MSWD = 2.8; Figure 6). Beside this, there is a clear pattern of discordance comprising analysis from the dark mantles (Figures 5c) that yields a lower intercept age at 326 ± 3 Ma (n = 8; MSWD = 1.15; prob. of fit = 0.33; Figure 6).

5.2 | Sample DGP-02: Lys-Caillaouas granitoid

CL images show euhedral zircon grains with double-ended prismatic or bipyramid shapes when unbroken (Figure 4a). Based on the CL features, two types of zircon grains can be distinguished. One group, called type-I zircon, shows bright cores and dark oscillatory-zoned mantles containing both prismatic and bipyramid shapes (Figure 4a). Some of the mantles cut the growth zoning in the cores, implying dissolution and reprecipitation during the formation of the mantles (e.g., Figure 4a, z5 and z25). The other group, called type-II zircon, consists of prismatic dark zircon with no differentiated cores that rarely developed dark unzoned tips (Figure 4a). We made 40 analyses, 20 in the bright cores, 4 in the dark oscillatory-zoned mantles, and 16 in the type-II zircon (see Table 2), with 34 out of 40 analyses falling within the ±5% of discordance (Figure 5d). Zircon grains show moderate U-contents, mostly below 1,500 ppm. Both zircon types show similar U-contents (medians of 521 and 610 ppm, respectively). The type-I zircon mantles show slightly higher U-content values (Figure 5b), but this could be an artefact due to a very small sample size for this zircon domain (n = 4). The individual ages of the different zircon domains and types overlap, but the ages of type-II zircon are mostly younger than 300 Ma, while the range of ages in the type-I zircon is wider (Figure 5d). All zircon types and domains show similar Th/U ratios typical of magmatic zircon (Figure 5f).

The Wetherill plot displays a complex age pattern with two tight concordant zircon clusters (Figure 7). The older cluster, fully formed by type-I bright cores, yields a concordia age at 320 ± 3 Ma (n = 3; 2-sigma; MSDW = 3.3; Figure 7). The younger cluster, fully formed by the type-II zircon, yields a Concordia age at 297 ± 2 Ma (n = 6; 2-sigma; MSWD = 2.8). In addition, the Concordia plot reveals two discordance patterns around the young tight cluster (Figure 7). One of them essentially consists of zircon analysis performed in the bright cores that along with zircon grains belonging to the younger cluster yields a lower intercept age at 298 ± 2 Ma (n = 11; MSWD = 0.83; prob. of fit = 0.60). The other is formed by a mix of type-I dark mantles and type-II zircon, yielding an upper intercept age similar to those obtained above (ca. 300 Ma). However, despite the good fit (n = 12; prob. of fit = 0.95), the error obtained is large due to the regression line intersecting the concordia curve at a very low angle.

6 | DISCUSSION

6.1 | Age of Bossòst and Lys-Caillaouas granitoids

Zircon grains in the Bossòst and Lys-Caillaouas granitoids have in common complex age patterns and two interpretable ages: one early Permian (293–299 Ma) and the other Serpukhovian–Bashkirian (Late Mississippian–Early Pennsylvanian; 317–329 Ma).

In the Lys-Caillaouas granitoid, type-II zircon grains show features typical of magmatic zircon and yield an age of 297 ± 2 Ma. This early Permian age represents, therefore, the age of crystallization of the Lys-Caillaouas leucogranitic facies. This age also agrees with those obtained by Esteban et al. (2015) in the basic (299 ± 1 Ma) and the porphyritic facies (300 ± 2 Ma), indicating that all the granite facies were emplaced in a very short period. Accordingly, we consider zircon with early Carboniferous ages (ca. 320 ± 2 Ma) as xenocrysts. In fact, all of them come from the analyses performed in the type-I zircon cores, and thus, these cores represent old zircon grains incorporated in the Permian magmatic event. Regarding the early Permian intercept ages, the upper intercept suggests a Pb-loss effect in some Permian zircon, while the lower intercept suggests either a core-rim mixing, a Pb-loss effect, or a combination of both in the inherited zircon grains.

The Bossòst granitoid only provides one concordant tight cluster that yields an early Permian age of 295 ± 4 Ma. This age is similar within the error to the age found in the Lys-Caillaouas granitoid and most likely represents the crystallization age of the Bossòst leucogranitic facies. This crystallization age is incompatible with the Visean ages obtained by Mezger and Gerdes (2016) in different facies of the Bossòst granitoid. The fact that we obtained this Permian age from zircon mantles with Th/U ratios typical of metamorphic zircon

TABLE 1 LA-ICP-MS U–Th–Pb data (sample DGP-01) for zircons from the Bossòst granitoid

Data point[a]	Domain	U[b] (ppm)	Th[b] (ppm)	Th/U	$^{207}Pb/^{206}Pb$[c]	±1σ	$^{207}Pb/^{235}U$[c]	±1σ	$^{206}Pb/^{238}U$[c]	±1σ	Rho	$^{208}Pb/^{232}Th$[c]	±1σ	% disc[d]	$^{206}Pb/^{238}U$	±1σ	$^{207}Pb/^{235}U$	±1σ	$^{207}Pb/^{206}Pb$	±1σ	$^{208}Pb/^{232}Th$	±1σ	Best age (Ma)	±1σ[a]
Zircon_22	Mantle–core?	40,748	75	0.002	0.05064	0.00122	0.25318	0.00806	0.03626	0.00059	0.790	0.01143	0.00766	0	230	4	229	7	224	52	230	153	230	4
Zircon_31	Mantle	154,529	534	0.003	0.04977	0.00045	0.29567	0.00543	0.04307	0.00069	0.870	0.02504	0.00075	−3	272	4	263	4	184	20	500	15	272	4
Zircon_36	Core	18,231	32	0.002	0.05090	0.00203	0.30398	0.01461	0.04331	0.00077	0.790	0.01364	0.01856	−1	273	5	270	11	236	86	274	370	273	5
Zircon_5	Core	81,598	233	0.003	0.05366	0.00070	0.33642	0.00668	0.04563	0.00068	0.750	0.19282	0.01099	2	288	4	294	5	357	27	3,564	186	288	4
Zircon_7	Mantle	7,345	3	0.000	0.05226	0.00050	0.32947	0.00360	0.04572	0.00022	0.490	0.01435	0.00581	0	288	1	289	3	297	23	288	116	288	1
Zircon_17	Core	87,586	262	0.003	0.05028	0.00047	0.31998	0.00511	0.04626	0.00060	0.810	0.04096	0.00164	−4	292	4	282	4	208	20	811	32	292	4
Zircon_37	Mantle	26,845	40	0.002	0.05276	0.00062	0.33991	0.00461	0.04672	0.00029	0.550	0.01465	0.00589	1	294	2	297	3	319	25	294	117	294	2
Zircon_8	Mantle	21,704	19	0.001	0.05262	0.00054	0.34002	0.00389	0.04687	0.00022	0.480	0.01470	0.00545	1	295	1	297	3	312	24	295	109	295	1
Zircon_27	Mantle	2,271	1	0.000	0.05292	0.00056	0.34107	0.00405	0.04675	0.00023	0.460	0.01465	0.02175	1	295	1	298	3	325	22	294	433	295	1
Zircon_13	Mantle–core?	12,228	13	0.001	0.05429	0.00136	0.35900	0.00958	0.04796	0.00031	0.430	0.01499	0.02596	3	302	2	311	7	383	58	301	517	302	2
Zircon_40	Mantle	28,403	47	0.002	0.05421	0.00185	0.36451	0.01530	0.04877	0.00085	0.690	0.01524	0.01871	3	307	5	316	11	380	72	306	373	307	5
Zircon_35	Mantle–core?	37,493	64	0.002	0.05343	0.00059	0.36317	0.00457	0.04913	0.00030	0.480	0.29523	0.02421	2	309	2	315	3	347	23	5,229	378	309	2
Zircon_28	Core	56,802	244	0.004	0.05757	0.00058	0.39419	0.00678	0.04984	0.00070	0.810	0.28845	0.02279	7	314	4	337	5	513	23	5,123	358	314	4
Zircon_10	Mantle–core?	38,327	117	0.003	0.05740	0.00063	0.39643	0.00617	0.05013	0.00055	0.710	0.31364	0.01756	7	315	3	339	4	507	22	5,514	270	315	3
Zircon_33	Core	62,014	163	0.003	0.05440	0.00060	0.38301	0.00547	0.05115	0.00047	0.640	0.23065	0.01522	2	322	3	329	4	388	23	4,195	250	322	3
Zircon_21	Mantle	15,161	21	0.001	0.05770	0.00255	0.40869	0.01930	0.05137	0.00049	0.400	0.01594	0.03495	7	323	3	348	14	518	91	320	695	323	3
Zircon_25	Mantle	26,029	55	0.002	0.05345	0.00101	0.37945	0.00832	0.05149	0.00046	0.570	0.01612	0.00647	1	324	3	327	6	348	40	323	129	324	3
Zircon_12	Mantle–core?	19,395	49	0.003	0.07835	0.00212	0.55532	0.01664	0.05166	0.00067	0.430	1.63290	0.11757	27	325	4	448	11	1,156	50	19,567	903	325	4
Zircon_3	Mantle–core?	35,094	90	0.003	0.07505	0.00180	0.55886	0.01746	0.05180	0.00104	0.640	1.63820	0.12942	28	326	6	451	11	1,070	45	19,608	992	326	6
Zircon_24	Mantle	52,642	320	0.006	0.05255	0.00148	0.37666	0.01141	0.05199	0.00043	0.400	0.01631	0.00340	−1	327	3	325	8	309	60	327	68	327	3
Zircon_1	Mantle	5,064	5	0.001	0.05806	0.00306	0.42022	0.02342	0.05250	0.00049	0.360	0.01627	0.04957	7	330	3	356	17	532	121	326	986	330	3
Zircon_29	Core	32,738	51	0.002	0.05488	0.00055	0.40079	0.00564	0.05271	0.00052	0.700	0.41858	0.01967	3	331	3	342	4	407	21	7,067	280	331	3
Zircon_9	Mantle	17,509	30	0.002	0.06365	0.00293	0.46347	0.02277	0.05281	0.00057	0.410	0.01620	0.03560	14	332	3	387	16	730	102	325	708	332	3
Zircon_38	Mantle	18,133	36	0.002	0.07098	0.00121	0.51911	0.01285	0.05285	0.00095	0.730	1.60760	0.13986	22	332	6	425	9	957	32	19,372	1,084	332	6
Zircon_14	Mantle	15,595	31	0.002	0.05291	0.00047	0.39272	0.00619	0.05390	0.00070	0.830	0.04450	0.00142	−1	338	4	336	5	325	19	880	27	338	4
Zircon_30	Mantle–core?	24,104	59	0.002	0.05302	0.00080	0.41456	0.01036	0.05606	0.00112	0.800	0.24312	0.03647	0	352	7	352	7	330	32	4,399	593	352	7
Zircon_26	Mantle	16,917	38	0.002	0.05305	0.00053	0.41298	0.00568	0.05646	0.00049	0.710	0.01769	0.00344	−1	354	3	351	4	331	21	355	68	354	3

(Continues)

TABLE 1 (Continued)

Data point[a]	Domain	U[b] (ppm)	Th[b] (ppm)	Th/U	$^{207}Pb/^{206}Pb^{c}$	±1σ	$^{207}Pb/^{235}U^{c}$	±1σ	$^{206}Pb/^{238}U^{c}$	±1σ	Rho	$^{208}Pb/^{232}Th^{c}$	±1σ	% disc[d]	$^{206}Pb/^{238}U$	±1σ	$^{207}Pb/^{235}U$	±1σ	$^{207}Pb/^{206}Pb$	±1σ	$^{208}Pb/^{232}Th$	±1σ	Best age (Ma)	±1σ[a]
Zircon_2	Mantle–core?	19,126	35	0.002	0.05265	0.00048	0.42022	0.00565	0.05793	0.00057	0.740	0.04978	0.00154	−2	363	3	356	4	314	19	982	30	363	3
Zircon_19	Core	64,701	201	0.003	0.06380	0.00089	0.52952	0.01250	0.05881	0.00112	0.810	0.91370	0.06579	15	368	7	431	8	735	28	13,119	695	368	7
Zircon_16	Mantle–core?	3,134	7	0.002	0.08103	0.00162	0.67641	0.01866	0.06084	0.00116	0.690	4.74030	0.33656	27	381	7	525	11	1,222	37	35,321	1,185	294	7
Zircon_15	Core	44,610	153	0.003	0.05592	0.00067	0.47965	0.00884	0.06245	0.00087	0.760	0.27322	0.01639	2	391	5	398	6	449	25	4,882	260	391	5
Zircon_18	Core	20,814	46	0.002	0.05568	0.00052	0.58738	0.00846	0.07630	0.00084	0.760	0.39989	0.01120	−1	474	5	469	5	440	19	6,799	162	474	5
Zircon_20	Mantle	30,488	129	0.004	0.05420	0.00054	0.57073	0.01077	0.07659	0.00123	0.850	0.17902	0.00859	−4	476	7	458	7	379	21	3,329	147	476	7

[a]Sample analysed July 2010 on the LEI-UNAM LA-ICP-MS.

[b]U and Th concentrations (ppm) are calculated relative to analyses of trace-element glass standard NIST 612.

[c]Isotopic ratios corrected relative to Plešovice standard zircon (Sláma et al., 2008). Common Pb corrections made using the Andersen (2002) method.

[d]Percentage discordance obtained using the following equation (100^{*} [(age^{207}Pb/^{235}U) – (age^{206}Pb/^{238}U)]/age^{207}Pb/^{235}U). Positive and negative values indicate normal and inverse discordance, respectively.

(Hoskin & Black, 2000; Rubatto, 2002; Williams & Claesson, 1987) might suggest that we dated a metamorphic instead of the crystallization event. However, we discard this hypothesis based on the following reasoning:

- Despite being uncommon, low (<0.1) Th/U ratios in magmatic zircon have been reported elsewhere (e.g., Ladenberger et al., 2014; Lopez-Sanchez, Aleinikoff, Marcos, Martínez, & Llana-Fúnez, 2016; Schärer, 1984; Zeck & Whitehouse, 1999). In fact, they are rather common in peraluminous granitoids that enclose zircon with U-content above 1,000 ppm (see figure 5 in Lopez-Sanchez et al., 2016), as it occurs in the sample dated.
- Zircon cores have similar low Th/U ratios (Figure 5e). Consequently, if the Th/U ratio is used as a condition to discriminate between magmatic and metamorphic origin, all the zircon enclosed in the granite sample must be regarded as metamorphic in origin, which is unlikely.
- The Visean zircon grains found by Mezger and Gerdes (2016) are completely different from those obtained in this study. Indeed, with the exception of zircon obtained from a granite sill, their appearance and Th/U ratios are completely different from ours. Furthermore, all zircon reported by Mezger and Gerdes (2016) show lower U contents. All this suggests that the early Carboniferous and the early Permian zircon comes from different magmatic events.

Based on the above considerations, we think that the leucogranitic facies of the Bossòst granitoid crystallized at early Permian times. Accordingly, the lower intercept that yields an early Carboniferous age suggests an early Carboniferous thermal event imprinted in pre-Variscan zircon. Strictly based on the available zircon U–Pb data, the question whether the main magmatic event and the concurrent HT metamorphism in the Garona dome is early Permian or Visean remains unsettled. Our data, however, confirm the need to carry out a detailed study of the different granite facies and their structural relationships to set a reliable relationship between the HT-LP metamorphisms event and the crystallization of the different facies of the Bossòst granitoid.

When U–Pb ages from the main metamorphic domes along the Axial Zone are compared (Table 3), the Lys-Caillaouas and the Canigou-Carançà domes are the only ones that present deep-seated granitoids with conclusive late Carboniferous to early Permian ages. In contrast, the Garona and Aston domes provide both early Carboniferous and late Carboniferous to early Permian zircon. In the Garona Dome, the different facies of the Bossòst granitoid provide both ages. In contrast, two different granitoids separated more than 20 km apart provide the different ages in the Aston Dome, the Soulcem (Mezger & Gerdes, 2016) and the Ax-les-Thermes (Denèle et al., 2014) granitoids, respectively. Mezger and Regnier (2016) have proposed two hypotheses to explain this age disparity across the domes: (i) the deep-seated granitoids, the HT-LP metamorphism, and related flat-lying schistosity are of Visean age only or (ii) the emplacement of deep-seated granitoids are diachronous across the Axial Zone, ranging from Visean in the central part to late Carboniferous in the eastern Axial Zone.

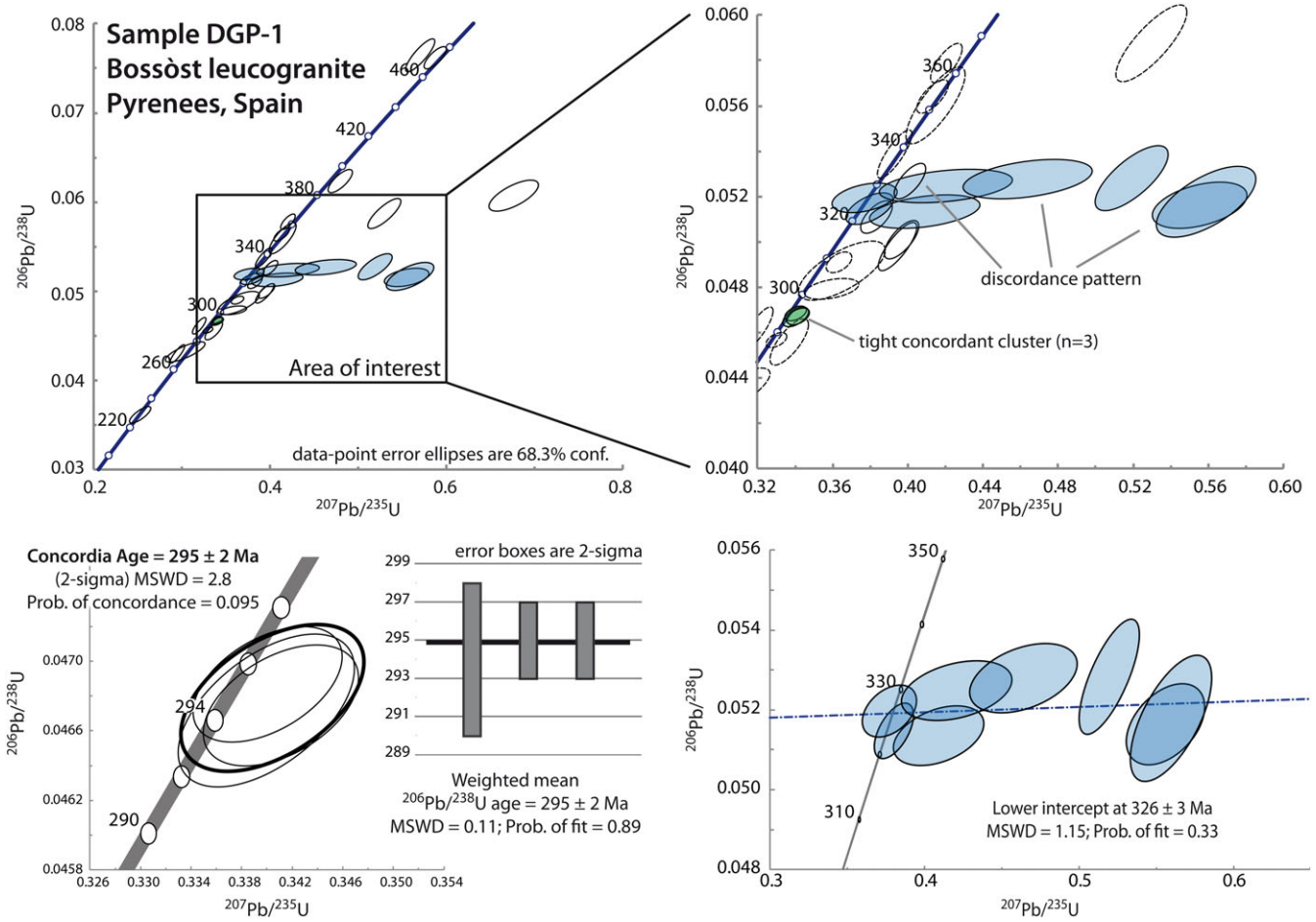

FIGURE 6 Wetherill and weighted average plots showing the different zircon dates in the sample DGP-01. Filled error ellipses are the ones used to estimate the different Concordia and intercept ages. Error ellipses and boxes are 2σ [Colour figure can be viewed at wileyonlinelibrary.com]

Our U–Pb zircon data discard both premises since the Lys-Caillaouas granitoid is located in the central part of the Axial Zone and provides a reliable U–Pb early Permian crystallization age.

6.2 | Potential sources for the early Carboniferous zircon grains in the Axial Zone

Visean–Bashkirian zircon grains appear frequently as inherited ages in most of the granitoids that outcrop within the metamorphic domes along the Pyrenees, including those studied here. Some igneous bodies have been dated as Serpukhovian (e.g., Martínez et al., 2008; Mezger & Gerdes, 2016), and migmatization in the Aston dome has been tentatively dated between 340 and 320 Ma (Mezger & Gerdes, 2016). Furthermore, Martínez et al. (2016) found zircon grains with Visean–Bashkirian ages in flysches along the adjacent Catalan Coastal Ranges 80 km south of the Pyrenean Axial Zone (Figure 1). All these data point to a widespread early Carboniferous magmatic event. Yet, the magmatic bodies that produced early Carboniferous zircon populations in the Pyrenees remain elusive. In addition, this contrasts to what is observed in the Central-Iberian zone of the Variscan Iberian Massif, where the Visean magmatic activity and the related magmatic bodies are well constrained (e.g., Gutiérrez-Alonso et al., 2018).

Biostratigraphic (Delvolvé, 1981; Delvolvé & Perret, 1989; Delvolvé, Souquet, Vachard, Perret, & Aguirre, 1993; Feist & Galtier, 1985; Sanz-López, Perret, & Vachard, 2006) and geochronological (detrital zircon population) data (Martínez et al., 2016) from syn-orogenic sedimentation (Culm deposits) in the Pyrenees, Montagne Noire, and Catalan Coastal Ranges indicate that Variscan deformation was active at least during the 360 to 315–310 Ma period (Tournaisian–Bashkirian). Hence, a probable cause for the origin of early Carboniferous zircon in the Pyrenees is a magmatic event due to thermal relaxation, which produced small segregated igneous bodies and the local migmatization in deep zones of the crust during the Variscan collision. This is in line with what Gutiérrez-Alonso et al. (2018) recently proposed for the adjacent Iberian (Variscan) Massif. The age of migmatization inferred by Mezger and Gerdes (2016) in the Aston dome, between 340 and 320 Ma, agrees with this hypothesis. Similarly, the Bashkirian ages (ca. 319 Ma) recently found in the Louzas granite and their related migmatites in the adjacent Variscan Montagne Noire (Poujol et al., 2017) support this hypothesis. The overprint of the widespread late Carboniferous to early Permian magmatism would explain the difficulty of finding and dating early Carboniferous magma bodies in situ in the Axial Zone. Compared to the Iberian Massif, it appears that the outcrop of the areas of the crust affected by this event is more limited in the Axial Zone or that the early Carboniferous magmatism was significantly less voluminous, making it more difficult to recognize.

TABLE 2 LA-ICP-MS U-Th-Pb data (sample DGP-01) for zircons from the Lys-Caillaouas granitoid

Data point[a]	Domain	U[b] (ppm)	Th[b] (ppm)	Th/U	$^{207}Pb/^{206}Pb$[c]	±1σ	$^{207}Pb/^{235}U$[c]	±1σ	$^{206}Pb/^{238}U$[c]	±1σ	Rho	$^{208}Pb/^{232}Th$[c]	±1σ	% disc[d]	$^{206}Pb/^{238}U$	±1σ	$^{207}Pb/^{235}U$	±1σ	$^{207}Pb/^{206}Pb$	±1σ	$^{208}Pb/^{232}Th$	±1σ	Best age (Ma)	±1σ[a]
Zircon_**36**	Dark mantle	2,132	374	0.18	0.05412	0.00054	0.27709	0.00367	0.03705	0.00032	0.660	0.01449	0.00017	5	235	2	248	3	376	21	291	3	235	2
Zircon_**31**	Dark Zr	1,967	125	0.06	0.05246	0.00063	0.28931	0.00412	0.04000	0.00027	0.540	0.01255	0.00009	2	253	2	258	3	306	26	252	2	253	2
Zircon_**14**	Bright core	1,637	1,409	0.86	0.05900	0.00153	0.35011	0.01033	0.04304	0.00028	0.360	0.01332	0.00008	11	272	2	305	8	567	59	267	2	272	2
Zircon_**30**	Dark Zr	1,094	722	0.66	0.05165	0.00094	0.30688	0.00669	0.04309	0.00026	0.460	0.01355	0.00007	0	272	2	272	5	270	39	272	1	272	2
Zircon_**17**	Dark Zr	1,184	1,171	0.99	0.05310	0.00052	0.32457	0.00368	0.04422	0.00026	0.500	0.01361	0.00014	2	279	2	285	3	333	23	273	3	279	2
Zircon_**15**	Dark Zr	514	329	0.64	0.05453	0.00071	0.33888	0.00504	0.04503	0.00032	0.480	0.01366	0.00019	4	284	2	296	4	393	31	274	4	284	2
Zircon_**6**	Dark Zr	617	187	0.30	0.05433	0.00103	0.33803	0.00721	0.04512	0.00029	0.350	0.01410	0.00009	4	285	2	296	5	385	40	283	2	285	2
Zircon_**7**	Dark mantle	508	457	0.90	0.05317	0.00074	0.33659	0.00515	0.04584	0.00028	0.420	0.01394	0.00015	2	289	2	295	4	336	30	280	3	289	2
Zircon_**24**	Dark Zr	773	349	0.45	0.05389	0.00059	0.34082	0.00416	0.04579	0.00024	0.440	0.01428	0.00016	3	289	1	298	3	366	26	287	3	289	1
Zircon_**21**	Dark mantle	937	313	0.33	0.05307	0.00071	0.33825	0.00557	0.04623	0.00028	0.510	0.01449	0.00008	2	291	2	296	4	332	32	291	2	291	2
Zircon_**26**	Bright core?	317	213	0.67	0.05428	0.00103	0.34612	0.00689	0.04627	0.00027	0.300	0.01444	0.00019	3	292	2	302	5	383	45	290	4	292	2
Zircon_**4**	Bright core	591	398	0.67	0.05420	0.00070	0.34969	0.00496	0.04671	0.00027	0.410	0.01423	0.00016	3	294	2	304	4	379	28	286	3	294	2
Zircon_**12**	Bright core	267	177	0.66	0.06182	0.00190	0.39768	0.01352	0.04665	0.00034	0.310	0.01436	0.00010	14	294	2	340	10	668	70	288	2	294	2
Zircon_**13**	Bright core	246	114	0.47	0.05656	0.00085	0.36563	0.00645	0.04669	0.00043	0.520	0.01474	0.00021	7	294	3	316	5	474	35	296	4	294	3
Zircon_**1**	Dark Zr	602	424	0.70	0.05316	0.00090	0.34353	0.00622	0.04675	0.00029	0.350	0.01382	0.00018	2	295	2	300	5	336	36	277	4	295	2
Zircon_**32**	Dark Zr	936	110	0.12	0.05289	0.00060	0.34209	0.00479	0.04691	0.00032	0.550	0.01471	0.00010	1	296	2	299	4	324	24	295	2	296	2
Zircon_**38**	Dark Zr	435	346	0.80	0.05374	0.00064	0.34890	0.00475	0.04703	0.00030	0.480	0.01429	0.00016	3	296	2	304	4	360	25	287	3	296	2
Zircon_**9**	Dark Zr	272	287	1.05	0.05316	0.00069	0.34704	0.00506	0.04722	0.00031	0.460	0.01434	0.00016	2	297	2	302	4	336	28	288	3	295	2
Zircon_**8**	Dark Zr	908	993	1.09	0.05163	0.00067	0.33789	0.00482	0.04734	0.00028	0.420	0.01444	0.00016	−1	298	2	296	4	269	28	290	3	296	2
Zircon_**10**	Bright core	162	64	0.39	0.05527	0.00094	0.36156	0.00662	0.04735	0.00032	0.370	0.01465	0.00021	5	298	2	313	5	423	40	294	4	298	2
Zircon_**2**	Dark Zr	290	157	0.54	0.05233	0.00094	0.34341	0.00662	0.04747	0.00033	0.360	0.01453	0.00017	0	299	2	300	5	300	43	292	3	295	2
Zircon_**16**	Dark Zr	404	214	0.53	0.05280	0.00069	0.34595	0.00494	0.04740	0.00028	0.400	0.01434	0.00016	1	299	2	302	4	320	31	288	3	296	2
Zircon_**33**	Bright core	521	283	0.54	0.05415	0.00065	0.35405	0.00477	0.04740	0.00029	0.450	0.01410	0.00017	3	299	2	308	4	377	26	283	3	299	2
Zircon_**34**	Dark Zr	564	490	0.87	0.05367	0.00070	0.35450	0.00505	0.04785	0.00028	0.400	0.01415	0.00017	2	301	2	308	4	357	28	284	3	301	2

(Continues)

TABLE 2 (Continued)

Data point[a]	Domain	U[b] (ppm)	Th[b] (ppm)	Th/U	$^{207}Pb/^{206}Pb$[c]	±1σ	$^{207}Pb/^{235}U$[c]	±1σ	$^{206}Pb/^{238}U$[c]	±1σ	Rho	$^{208}Pb/^{232}Th$[c]	±1σ	% disc[d]	$^{206}Pb/^{238}U$	±1σ	$^{207}Pb/^{235}U$	±1σ	$^{207}Pb/^{206}Pb$	±1σ	$^{208}Pb/^{232}Th$	±1σ	Best age (Ma)	±1σ[a]
Zircon_**39**	Bright core	917	294	0.32	0.05287	0.00053	0.35210	0.00412	0.04824	0.00029	0.520	0.01423	0.00020	1	304	2	306	3	323	22	286	4	304	2
Zircon_**3**	Dark Zr	348	158	0.45	0.05254	0.00074	0.35854	0.00607	0.04945	0.00047	0.550	0.01503	0.00024	0	311	3	311	5	309	34	302	5	311	3
Zircon_**23**	Bright core	245	146	0.60	0.05494	0.00077	0.37791	0.00574	0.04990	0.00029	0.390	0.01504	0.00018	3	314	2	325	4	410	33	302	4	314	2
Zircon_**28**	Bright core	492	236	0.48	0.05373	0.00064	0.37635	0.00519	0.05078	0.00035	0.500	0.01562	0.00020	2	319	2	324	4	360	28	313	4	319	2
Zircon_**11**	Bright core	359	170	0.47	0.05805	0.00130	0.40753	0.01019	0.05092	0.00031	0.350	0.01579	0.00009	8	320	2	347	7	532	52	317	2	320	2
Zircon_**37**	Bright core	350	192	0.55	0.05304	0.00080	0.37341	0.00625	0.05097	0.00038	0.430	0.01482	0.00019	1	320	2	322	5	331	32	297	4	319	2
Zircon_**25**	Bright core	626	396	0.63	0.05359	0.00080	0.37897	0.00679	0.05113	0.00050	0.550	0.01448	0.00017	2	321	3	326	5	354	36	291	3	319	2
Zircon_**19**	Bright core	683	50	0.07	0.05242	0.00071	0.38421	0.00663	0.05316	0.00047	0.630	0.01668	0.00019	−1	334	3	330	5	304	32	334	4	334	3
Zircon_**35**	Bright core	1,206	122	0.10	0.05478	0.00058	0.40695	0.00603	0.05388	0.00048	0.670	0.01682	0.00015	3	338	3	347	4	403	22	337	3	338	3
Zircon_**27**	Dark mantle	1,074	94	0.09	0.05849	0.00060	0.53577	0.00657	0.06643	0.00038	0.530	0.02058	0.00013	5	415	2	436	4	548	24	412	3	415	2
Zircon_**20**	Bright core	655	502	0.77	0.05887	0.00065	0.60345	0.00800	0.07417	0.00055	0.550	0.02518	0.00028	4	461	3	479	5	562	25	503	6	461	3
Zircon_**5**	Bright core	792	280	0.35	0.05986	0.00060	0.67954	0.00896	0.08222	0.00071	0.650	0.02531	0.00030	3	509	4	526	5	599	21	505	6	509	4
Zircon_**29**	Bright core	619	400	0.65	0.05861	0.00058	0.69521	0.00872	0.08589	0.00066	0.610	0.02732	0.00036	1	531	4	536	5	553	23	545	7	531	4
Zircon_**18**	Bright core–mantle	289	171	0.59	0.06380	0.00083	0.87519	0.01284	0.09930	0.00068	0.460	0.03137	0.00044	4	610	4	638	7	735	29	624	9	610	4
Zircon_**40**	Bright core	828	134	0.16	0.09248	0.00088	1.47753	0.01778	0.11587	0.00072	0.590	0.03412	0.00024	23	707	4	921	7	1,477	17	678	5	1,477	17
Zircon_**22**	Dark Zr	880	112	0.13	0.18400	0.00149	7.17650	0.07683	0.28302	0.00198	0.650	0.04824	0.00063	25	1,607	10	2,134	10	2,689	14	952	12	2,689	14

[a]Sample analysed July 2010 on the LEI-UNAM LA-ICP-MS.

[b]U and Th concentrations (ppm) are calculated relative to analyses of trace-element glass standard NIST 612.

[c]Isotopic ratios corrected relative to Plešovice standard zircon (Sláma et al., 2008). Common Pb corrections made using the Andersen (2002) method.

[d]Percentage discordance obtained using the following equation (100^{*} [(age$^{207}Pb/^{235}U$) − (age$^{206}Pb/^{238}U$)]/age$^{207}Pb/^{235}U$). Positive and negative values indicate normal and inverse discordance, respectively.

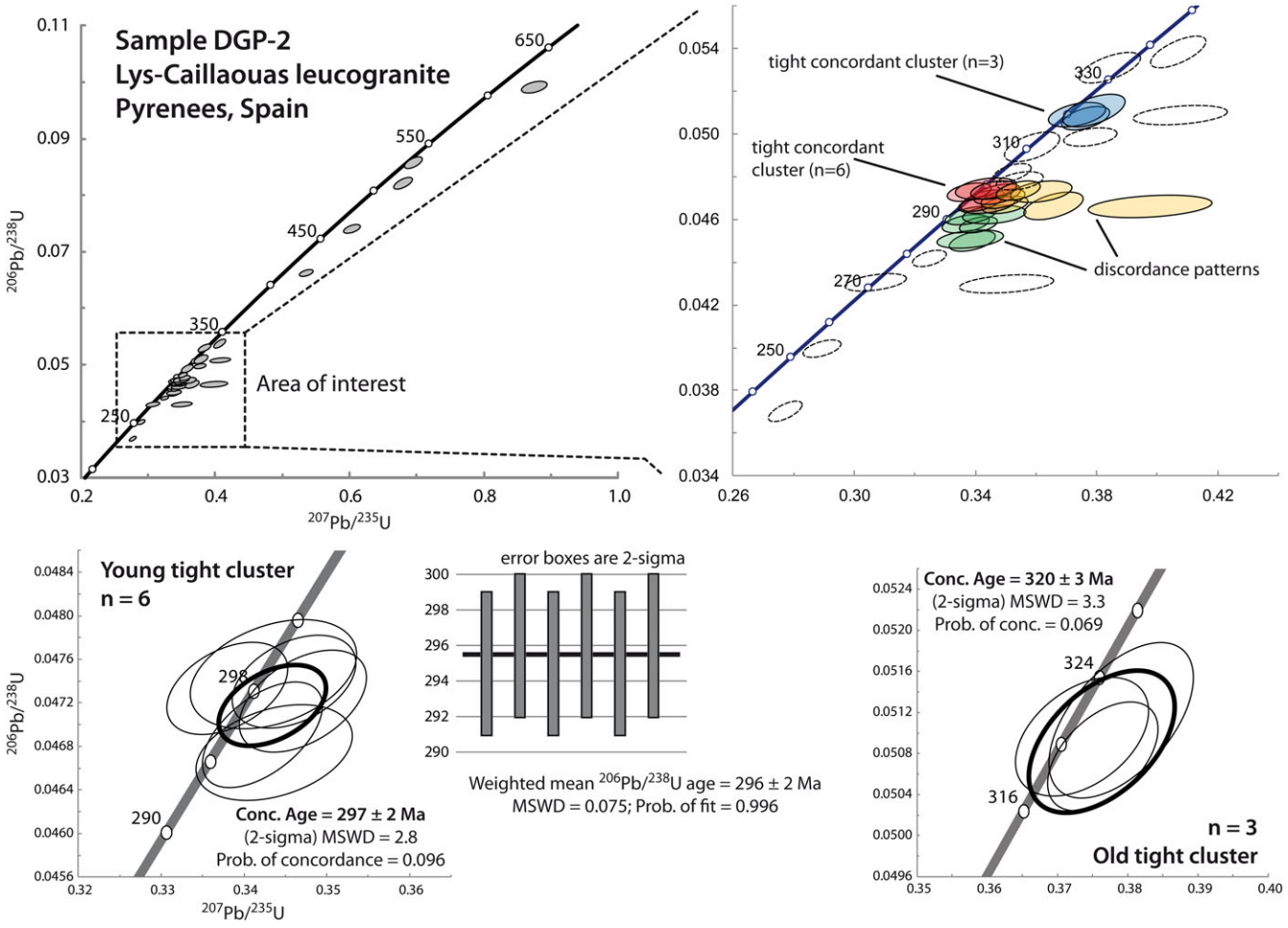

FIGURE 7 Wetherill and weighted average plots showing the different zircon dates in the sample DGP-02. Filled error ellipses are the ones used to estimate the different Concordia ages. Error ellipses and boxes are 2σ [Colour figure can be viewed at wileyonlinelibrary.com]

TABLE 3 U–Pb existing ages in the main metamorphic domes within the Axial zone

	Early Carboniferous				Late Carboniferous to early Permian			
Metamorphic dome	Num.	Age (Ma)	Method	Reference	Num.	Age (Ma)	Method	Reference
Lys-Caillaouas	1	320	Concordia zircon U–Pb[a]	This study	3	297	Concordia zircon U–Pb	This study
						299 300	Concordia zircon U–Pb	Esteban et al. (2015)
Garona	2	338 337	Concordia zircon U–Pb	Mezger and Gerdes (2016)	1	295	Concordia zircon U–Pb	This study
	1	326	Lower intercept U–Pb	This study				
Canigou-Carança	No found				1	305	Concordia zircon U–Pb	Denèle et al. (2014)
Aston	1	339	Concordia zircon U–Pb	Mezger and Gerdes (2016)	1	306	Lower intercept U–Pb	Denèle et al. (2014)
Hospitalet	No data				No data			

[a]Found in zircon cores and interpreted as inherited zircon grains (i.e., xenocrysts).

7 | CONCLUSIONS

Our data provide a crystallization age of 297 ± 2 Ma for the Lys-Caillaouas granitoid and, for the first time, an early Permian age of 295 ± 2 for the leucogranitic facies of the Bossòst granitoid. We also provide the first evidence of inherited zircon with early Carboniferous ages in the Lys-Caillaouas granitoid. Some discordant zircon grains in the Bossòst granitoid also suggest an early Carboniferous thermal

event recorded in pre-Variscan zircon. These data reinforce the idea that there was an elusive but widespread early Carboniferous magmatic event in the Pyrenees.

The crystallization age of Lys-Caillaouas granitoid establishes an early Permian age for the HT-LP metamorphism peak in the Lys-Caillaous Dome. This discards two previous hypotheses that tried to explain the disparity of ages across different metamorphic domes in the Axial Zone: (i) a general Visean age for the HT-LP metamorphism or (ii) the diachronic formation of domes along the Axial Zone, ranging from Visean in the central Axial Zone to late Carboniferous in the eastern Axial Zone. The early Permian age found in the leucogranitic facies of the Bossòst granitoid questions the Visean age for the formation of Garona Dome and the HT-LP metamorphism, as proposed by Mezger and Gerdes (2016), and points to an Early Permian age as most likely, in line with what is observed in the Lys-Caillaouas Dome.

ACKNOWLEDGEMENTS

This work was supported by the Spanish Ministry for Science and Innovation (Grant CGL2006-08822/BTE). A first review by Alberto Marcos helped to improve and focus the content of this manuscript. We thank Gabriel Gutiérrez-Alonso and an anonymous reviewer for improving the content and the focus in the manuscript. We thank Alexander Iriondo for taking care of zircon separation.

CONFLICTS OF INTEREST

The authors declare no conflict of interest.

ORCID

Marco A. Lopez-Sanchez http://orcid.org/0000-0002-0261-9267

REFERENCES

Aerden, D. G. A. M. (1994). Kinematics of orogenic collapse in the Variscan Pyrenees deduced from microstructures in porphyroblastic rocks from the Lys-Caillaouas Massif. *Tectonophysics*, *238*, 139–160.

Andersen, T. (2002). Correction of common lead in U-Pb analyses that do not report 204Pb. *Chemical Geology*, *192*, 59–79.

Autran, A., Fonteilles, M., & Guitard, G. (1970). Relations entre les intrusions de granitoides, l'anatexie et le metamorphisme regional considerees principalement du point de vue du role de l'eau; cas de la chaine hercynienne des Pyrenees orientales. *Bulletin de la Société Géologique de France*, *S7-XII*(4), 673–731.

Carreras, J., & Capella, I. (1994). Tectonic levels in the Palaeozoic basement of the Pyrenees: A review and a new interpretation. *Journal of Structural Geology*, *16*, 1509–1524.

Casas, J. M. (2010). Ordovician deformations in the Pyrenees: New insights into the significance of pre-Variscan ("sardic") tectonics. *Geological Magazine*, *147*, 647–689.

Cavet, P. (1957). Le Paléozoïque de la zone axiale des Pyrénées orientales françaises entre le Roussillon et l' Andorre (étude stratigraphique et paléontologique). *Bulletin des Services de la Carte géologique de France*, *254*, 303–518.

Clariana, P., & García-Sansegundo, J. (2009). Variscan structure in the eastern part of the Pallaresa massif, Axial Zone of the Pyrenees (NW Andorra). Tectonic implications. *Bulletin de la Société Géologique de France*, *180*(6), 501–511.

Clin, M. (1964). Étude géologique de la haute chaîne des Pyrénées centrales entre le cirque de Troumouse et le cirque de Lys. *Mémoires du Bureau de Recherches Géologiques et Minières*, *27*, 1–379.

Clin, M., Lelong, F., Poty, B., De La Roche, H., Fauré, J., Macaudière, J., … Blanquart, P. R. (1986). Carte géologique de la France à 1: 50.000, n° 1084, Bagnères de Luchon. In M. Clin, F. Taillefer, P. Pouchan, & A. P. Muller (Eds.), *Notice explicative de la feuille pour* (p. 80). Orléans: Bureau de Recherches Géologiques et Minières.

Delvolvé, J. J. (1981). Arguments en faveur de l' âge namurien du Culm des Pyrénées Centrales françaises. *Comptes Rendus de l' Academie des Sciences Serie II*, *293*(3), 219–222.

Delvolvé, J. J., & Perret, M. F. (1989). Variations de l' âge des sédiments calcaires et Culm Carbonifère dans la chaîne varisque du sud de la France: Migration de l' órogenèse varisque. *Geodinamica Acta*, *3*(2), 117–126.

Delvolvé, J. J., Souquet, P., Vachard, D., Perret, M. F., & Aguirre, P. (1993). Caractérisation d' un bassin d' avant-pays dans le Carbonifère des Pyrénées: faciès, chronologie de la tectonique synsédimentaire. *Comptes Rendus de l' Academie des Sciences Serie II*, *316*(7), 959–966.

Denèle, Y. (2007). *Formation des dômes gneissiques hercyniens dans les Pyrénées: exemple du massif de l'Aston-Hospitalet*. PhD Dissertation, Universite de Tolouse III, France.

Denèle, Y., Laumonier, B., Paquette, J. L., Olivier, P., Gleizes, G., & Barbey, P. (2014). Timing of granite emplacement, crustal flow and gneiss dome formation in the Variscan segment of the Pyrenees. *Geological Society of London, Special Publications*, *405*, 265–287.

Druguet, E., Castro, A., Chichorro, M., Francisco Pereira, M., & Fernandez, C. A. (2014). Zircon geochronology of intrusive rocks from Cap de Creus, Eastern Pyrenees. *Geological Magazine*, *151*(6), 1095–1114.

Esteban, J. J., Aranguren, A., Cuevas, J., Hilario, A., Tubia, J. M., Larionov, A., & Sergeev, S. (2015). Is there a time lag between the metamorphism and emplacement of plutons in the Axial Zone of the Pyrenees? *Geological Magazine*, *152*(5), 935–941.

Evans, N. G., Gleizes, G., Leblanc, D., & Bouchez, J. L. (1998). Syntectonic emplacement of the Maladeta granite (Pyrenees) deduced from relationships between Hercynian deformation and contact metamorphism. *Journal of the Geological Society*, *155*, 209–216.

Feist, R., & Galtier, J. (1985). Découverte de flores d'âge Namurien probable dans le flysch à olistolithes de Cabrières (Hérault). Implications sur la durée de la sédimentation synorogénique dans la Montagne Noire (France méridionale). *Comptes Rendues Academie Sciences Paris*, *300*, 207–212.

García-López, S., García-Sansegundo, J., & Arbizu, M. (1991). Devonian of the Aran Valley Synclinorium, Central Pyrenees, Spain: Stratigraphical and paleontological data. *Acta Geológica Hispánica*, *26*(1), 55–66.

García-Sansegundo, J. (1990). Structure of the Paleozoic in the Aran Valley, Axial Zone, Central Pyrenees. *Bulletin de la Société Géologique de France*, *6*(2), 229–239.

García-Sansegundo, J. (1992). Estratigrafía y Estructura de la Zona Axial Pirenaica en la transversal del Valle de Arán y de la Alta Ribagorça. *Publicaciones especiales del Boletín Geológico y Minero*, *102-103*, 1–167.

García-Sansegundo, J. (1996). Hercynian structure of the Axial Zone of the Pyrenees: The Aran Valley cross-section (Spain-France). *Journal of Structural Geology*, *18*(11), 1315–1325.

García-Sansegundo, J., & Alonso, J. L. (1989). Stratigraphy and Structure of the southeastern Garona Dome. *Geodinamica Acta*, *3*(2), 127–134.

García-Sansegundo, J., Gavaldà, J., & Alonso, J. L. (2004). Preuves de la discordance de l' Ordovicien supérieur dans la Zone Axiale des Pyrénées: exemple du Dôme de la Garonne (Espagne, France). *Comptes Rendus Geoscience*, *336*(11), 1035–1040.

García-Sansegundo, J., Martín-Izard, A., & Gavaldà, J. (2014). Structural control and geological significance of the Zn-Pb ores formed in the Benasque Pass area (Central Pyrenees) during the post-late Ordovician extensional event of the Gondwana margin. *Ore Geology Reviews*, *56*, 516–527.

García-Sansegundo, J., Poblet, J., Alonso, J. L., & Clariana, P. (2011). Hinterland-foreland zonation of the Variscan orogen in the Central Pyrenees: Comparison with the northern part of the Iberian Variscan Massif. *Geological Society of London, Special Publications*, *349*, 169–184.

García-Sansegundo, J., & Ramírez Merino, J. I. (2013). *Mapa Geológico de España E. 1:50.000, Hoja n° 118bis-148 (Caneján-Viella), 2ª Serie MAGNA*. Madrid: Instituto Geológico y Minero de España.

Gehrels, G. E., Valencia, V. A., & Ruiz, J. (2008). Enhanced precision, accuracy, efficiency, and spatial resolution of U-Pb ages by laser ablation-multicollector-inductively coupled plasma-mass spectrometry. *Geochemistry Geophysics Geosystems*, *9*(3), Q03017.

Gleizes, G., Crevon, G., Asrat, A., & Barbey, P. (2006). Structure, age and mode of emplacement of the Hercynian Borderes-Louron pluton (Central Pyrenees, France). *International Journal of Earth Sciences*, *95*(6), 1039–1052.

Gutiérrez-Alonso, G., Fernández-Suárez, J., López-Carmona, A., & Gärtner, A. (2018). Exhuming a cold case: The early granodiorites of the northwest Iberian Variscan belt—A Visean magmatic flare-up? *Lithosphere* https://doi.org/10.1130/L706.1, *10*, 194–216.

Gutiérrez-Medina, M., Alonso, J. L., & García-Sansegundo, J. (2012). Reconstrucción de la estructura varisca mediante la retrodeformación de una secuencia permo-triásica discordante, deformada por la reactivación de pliegues variscos. *Zona Axial Pirenaica*. *Geo-Temas*, *13*, 389–392.

Hilario, A. (2004). *Relaciones entre magmatismo y deformación en la transversal de Benasque a Luchon (Zona Axial del Pirineo)*. PhD Dissertation, Departamento de Geodinámica, Universidad del País Vasco, España.

Hoskin, P. W. O., & Black, L. P. (2000). Metamorphic zircon formation by solid-state recrystallization of protolith igneous zircon. *Journal of Metamorphic Geology*, *18*(4), 423–439.

Jackson, S. E., Longerich, H. P., Dunning, G. R., & Fryer, B. J. (1992). The application of laser-ablation microprobe; inductively coupled plasma-mass spectrometry (LAM-ICP-MS) to in situ trace-element determinations in minerals. *Canadian Mineralogist*, *30*, 1049–1064.

Kleinsmiede, W. F. J. (1960). Geology of the Valle de Arán (Central Pyrenees). *Leidse Geologische Mededelingen*, *25*, 129–245.

Kriegsman, L. M., Aerden, D. G. A. M., Bakker, R. J., Denbrok, S. W. J., & Schutjens, P. M. T. M. (1989). Variscan tectonometamorphic evolution of the eastern Lys-Caillaouas Massif, Central Pyrenees—Evidence for late orogenic extension prior to peak metamorphism. *Geologie en Mijnbouw*, *68*(3), 323–333.

Ladenberger, A., Be'eri-Shlevin, Y., Claesson, S., Gee, D. G., Majka, J., & Romanova, I. V. (2014). Tectonometamorphic evolution of the Åreskutan Nappe–Caledonian history revealed by SIMS U–Pb zircon geochronology. *Geological Society London, Special Publications*, *390*(1), 337–368.

López-Moro, F. J., López-Plaza, M., Gutiérrez-Alonso, G., Fernández-Suárez, J., López-Carmona, A., Hofmann, M., & Romar, R. L. (2018). Crustal melting and recycling: Geochronology and sources of Variscan syn-kinematic anatectic granitoids of the Tormes Dome (Central Iberian Zone). A U-Pb LA-ICP-MS study. *International Journal of Earth Sciences (Geol Rundsch)*, *107*, 1–20. https://doi.org/10.1007/s00531-017-1483-8.

Lopez-Sanchez, M. A., Aleinikoff, J. N., Marcos, A., Martínez, F. J., & Llana-Fúnez, S. (2016). An example of low-Th/U zircon overgrowths of magmatic origin in a late orogenic Variscan intrusion: The San Ciprian massif (NW Spain). *Journal of the Geological Society*, *173*(2), 282–291. https://doi.org/10.1144/jgs2015-071

Lopez-Sanchez, M. A., Marcos, A., Martínez, F. J., Iriondo, A., & Llana-Fúnez, S. (2015). Setting new constrains on the age of crustal-scale extensional shear zone (Vivero fault): Implications for the evolution of Variscan orogeny in the Iberian massif. *International Journal of Earth Sciences*, *104*, 927–962. https://doi.org/10.1007/s00531-014-1119-1

Ludwig, K. R. (2012). Isoplot 3.75—A geochronological toolkit for Microsoft Excel. Berkeley Geochronology Center, Special Publications 5.

Martínez, F. J., Dietsch, C. A., Aleinikoff, J. N., Cirés, J., Arboleya, M. L., Reche, J., & Gomez-Gras, D. (2016). Provenance, age, and tectonic evolution of Variscan flysch, southeastern France and northeastern Spain, based on zircon geochronology. *Geological Society of America Bulletin*, *128*(5–6), 842–859.

Martínez, F. J., Reche, J., & Iriondo, A. (2008). U-Pb Shrimp-RG zircon ages of Variscan igneous rocks from the Guilleries massif (NE Iberia pre-Mesozoic basement). Geological implications. *Comptes Rendus Geoscience*, *340*(4), 223–232.

Matte, P. (1969). Le problème du passage de la schistosité horizontale à la schistosité verticale dans le dôme de Garonne (Paléozoïque des Pyrénées Centrales). *Comptes Rendus Hebdomadaires des séances de l' Académie des Sciences Série D*, *268*(14), 1841–1844.

Maurel, O., Respaut, J. P., Monie, P., Arnaud, N., & Brunel, M. (2004). U-Pb emplacement and 40Ar/39Ar cooling ages of the eastern Mont-Louis granite massif (Eastern Pyrenees, France). *Comptes Rendus Geoscience*, *336*(12), 1091–1098.

Mey, P. H. W. (1968). Geology of the Upper Ribagorzana and Tor valleys, Central Pyrenees, Spain. *Leidse Geologische Mededelingen*, *41*, 229–292.

Mezger, J. E. (2009). Transpressional tectonic setting during the main Variscan deformation: Evidence from four structural levels in the Bossòst and Aston-Hospitalet mantled gneiss domes, central Axial Zone, Pyrenees. *Bulletin de la Société Géologique de France*, *180*(3), 199–207.

Mezger, J. E., & Gerdes, A. (2016). Early Variscan (Visean) granites in the core of central Pyrenean gneiss domes: Implications from laser ablation U-Pb and Th-Pb studies. *Gondwana Research*, *29*(1), 181–198.

Mezger, J. E., & Passchier, C. A. W. (2003). Polymetamorphism and ductile deformation of staurolite-cordierite schist of the Bossòst dome: Indication for Variscan extension in the Axial Zone of the central Pyrenees. *Geological Magazine*, *140*(5), 595–612.

Mezger, J. E., & Regnier, J. L. (2016). Stable staurolite–cordierite assemblages in K-poor metapelitic schists in Aston and Hospitalet gneiss domes of the central Pyrenees (France, Andorra). *Journal of Metamorphic Geology*, *34*, 167–190.

Paquette, J. L., Gleizes, G., Leblanc, D., & Bouchez, J. L. (1997). Le granite de Bassiès (Pyrénées): un pluton syntectonique d' âge westfalien. Géochronologie U-Pb sur zircons. *Comptes Rendus de l' Académie des Sciences Série II Fascicule A - Sciences de la Terre et des Planètes*, *324*(5), 387–392.

Paterson, S. R., & Tobisch, O. T. (1988). Using pluton ages to date regional deformations: Problems with commonly used criteria. *Geology*, *16*(12), 1108–1111.

Paterson, S. R., Tobisch, O. T., & Vernon, R. H. (1989). Criteria for establishing the relative timing of pluton emplacement and regional deformation. *Geology*, *17*(5), 475–476.

Pereira, M. F., Castro, A., Chichorro, M., Fernández, C. A., Díaz-Alvarado, J., Martí, J., & Rodríguez, C. A. (2014). Chronological link between deep-seated processes in magma chambers and eruptions: Permo-Carboniferous magmatism in the core of Pangaea (Southern Pyrenees). *Gondwana Research*, *25*(1), 290–308.

Pérez Cáceres, I., & García-Sansegundo, J. (2012). Estructura y metamorfismo de la Zona Axial pirenaica en el sector suroccidental del Macizo de Lys-Caillaouas (Huesca, España). *Geo-Temas*, *13*, 421–424.

Poilvet, J. C. A., Poujol, M., Pitra, P., Van Den Driessche, J., & Paquette, J. L. (2011). The Montalet granite, Montagne Noire, France: An Early Permian syn-extensional pluton as evidenced by new U-Th-Pb data on zircon and monazite. *Comptes Rendus Geoscience*, *343*, 454–461.

Poujol, M., Pitra, P., Van Den Driessche, J., Tratèse, R., Rufffet, G., Paquette, J.-L., & Poilvet, J.-C. A. (2017). Two-stage partial melting during the Variscan extensional tectonics (Montagne Noire, France). *International Journal of Earth Sciences*, *106*(2), 477–500.

Roberts, M. P., Pin, C. A., Clemens, J. D., & Paquette, J. L. (2000). Petrogenesis of mafic to felsic plutonic rock associations: The Calc-alkaline Querigut Complex, French Pyrenees. *Journal of Petrology*, *41*(6), 809–844.

Romer, R. L., & Soler, A. (1995). U-Pb age and lead isotopic characterization of Au-bearing skarn related to the Andorra Granite (Central Pyrenees, Spain). *Mineralium Deposita*, *30*(5), 374–383.

Rubatto, D. (2002). Zircon trace element geochemistry: Partitioning with garnet and the link between U-Pb ages and metamorphism. *Chemical Geology*, *184*(1–2), 123–138.

Sanz-López, J., Perret, M. F., & Vachard, D. (2006). Silurian to Mississippian series of the eastern Catalan Pyrenees (Spain), updated by conodonts, foraminifers and algae. *Geobios*, *39*(5), 709–725.

Schärer, U. (1984). The effect of initial 230Th disequilibrium on young UPb ages: The Makalu case, Himalaya. *Earth and Planetary Science Letters*, *67*(2), 191–204.

Schneider, C. A. A., Rasband, W. S., & Eliceiri, K. W. (2012). NIH Image to ImageJ: 25 years of image analysis. *Nature Methods*, *9*(7), 671–675.

Sláma, J., Košler, J., Condon, D. J., Crowley, J. L., Gerdes, A., Hanchar, J. M., … Whitehouse, M. J. (2008). Plešovice zircon—A new natural reference material for U-Pb and Hf isotopic microanalysis. *Chemical Geology*, *249*(1–2), 1–35.

Solari, L. A., Gomez-Tuena, A., Pablo Bernal, J., Perez-Arvizu, O., & Tanner, M. (2010). U-Pb zircon geochronology with an integrated LA-ICP-MS microanalytical workstation: Achievements in precision and accuracy. *Geostandards and Geoanalytical Research*, *34*(1), 5–18.

Solari, L. A., & Tanner, M. (2011). U-Pb age, a fast data reduction script for LA-ICP-MS U-Pb geochronology. *Revista Mexicana De Ciencias Geológicas*, *28*(1), 83–91.

Stacey, J. S., & Kramers, J. D. (1975). Approximation of terrestrial lead isotope evolution by a 2-stage model. *Earth and Planetary Science Letters*, *26*(2), 207–221.

Van Den Eeckhout, B., & Zwart, H. J. (1988). Hercynian crustal-scale extensional shear zone in the Pyrenees. *Geology*, *16*(2), 135–138.

Vissers, R. L. M. (1992). Variscan extension in the Pyrenees. *Tectonics*, *11*(6), 1369–1384.

Wetherill, G. W. (1956). Discordant uranium-lead ages. I. Transactions. *American Geophysical Union*, *37*(3), 320.

Williams, I. S., & Claesson, S. (1987). Isotopic evidence for the Precambrian provenance and Caledonian metamorphism of high grade paragneisses from the Seve Nappes, Scandinavian Caledonides. 2. Ion microprobe zircon U-Th-Pb. *Contributions to Mineralogy and Petrology*, *97*(2), 205–217.

Zeck, H. P., & Whitehouse, M. J. (1999). Hercynian, Pan-African, Proterozoic and Archean ion-microprobe zircon ages for a Betic-Rif core complex, Alpine belt, W Mediterranean—Consequences for its P-T-t path. *Contributions to Mineralogy and Petrology*, *134*(2–3), 134–149.

Zwart, H. J. (1963). Metamorphic history of the Central Pyrenees, Part II. Valle de Aran, sheet 4. *Leidse Geologische Mededelingen*, *28*, 321–376.

Zwart, H. J. (1979). The geology of the Central Pyrennes. *Leidse Geologische Mededelingen*, *50*, 1–74.

How to cite this article: Lopez-Sanchez MA, García-Sansegundo J, Martínez FJ. The significance of early Permian and early Carboniferous U–Pb zircon ages in the Bossòst and Lys-Caillaouas granitoids (Pyrenean Axial Zone). *Geological Journal*. 2018;1–16. https://doi.org/10.1002/gj.3283